PhotoniX

RESEARCH Open Access

Orthogonal GHz harmonic dual-comb generation in monolithic fiber cavity for acquisition speed multiplication

Guorui Wang[1†], Zixuan Ding[1†] and Fei Xu[1*]

†Guorui Wang and Zixuan Ding contributed equally to this work.

*Correspondence: feixu@nju.edu.cn

[1] College of Engineering and Applied Sciences and Collaborative Innovation Center of Advanced Microstructures, Nanjing University, Nanjing 210023, China

Abstract

Asynchronous dual-comb generated in single laser cavity offer potent tools for simplified coherent measurements, owing to the common mode rejection which spares the sophisticated locking systems. However, the limited dimensional inhomogeneity in monolithic cavity induces relatively small repetition-rate-difference, hindering high-speed measurements. Here, a monolithic linear fiber laser with integrated multifunctional device employing polarization multiplexing is proposed and demonstrated for dual-comb acquisition speed enhancement. By tuning the inherent polarization-dependent degrees of freedom within the device, optical intensity distribution between orthogonal polarizations can be finely manipulated, thus boosting controllable asynchronous harmonic mode-locking. The two sets of harmonic mode-locked pulses enable the multiplication of the equivalent repetition-rate-difference and produce more temporal interferograms via least common multiple principles. With a fundamental-repetition-rate of 383 MHz, harmonic-repetition-rate up to 2.3 GHz and acquisition speed over 244 kHz are obtained in experiments, faster by 2 orders of magnitudes than previous single-fiber-cavity dual-combs. Equivalent repetition-rate-difference up to 400 kHz is also achieved with shorter laser cavity. This orthogonally polarized GHz harmonic dual-comb laser offers insights for a novel dual-comb generation paradigm and provides a single-fiber-integrated solution for acquisition boosting in wide measurement applications.

Keywords: Harmonic mode-locking, Polarization multiplexing, Dual-combs, Monolithic cavity fiber lasers, High-repetition-rate-difference

Introduction

On the basis of optical frequency comb (OFC), the dual-comb technology has brought revolution to metrology by using two sets of OFCs with different repetition rates (f_{rep}) to achieve temporal asynchronous sampling and spectral multimode heterodyne interference, which drastically reduces the equipment bandwidth and enables measurements with concise acquisition and processing systems. Classical methods of acquiring dual-comb involve locking of two individual mode-locked lasers. Recent studies have shown that two stable mode-locked pulse trains can be generated in one oscillation cavity by exploiting diverse multiplexing dimensions, such as circulation directions, wavelengths,

cavity space, polarizations, and pulse waveforms. Both pulse trains experience same perturbation in the same cavity, ensuring effective common-mode noise suppression and high coherence without complex locking systems, thereby named as "single-cavity dual-comb".

With high adaptability and flexibility, fiber laser scheme has become one of the mainstream paths to form single-cavity dual-comb sources. Nevertheless, the f_{rep} of fiber-based cases are usually within tens of megahertz, with corresponding repetition rate difference (Δf_{rep}) within tens of hertz to a few kilohertz. Since the acquisition speed of dual-comb system being determined by the Δf_{rep}, such low levels could hamper applications in high-speed dynamic scenarios. In dual-comb ranging, the equivalent sampling rate depends on both the f_{rep} and the Δf_{rep}. Under the Nyquist sampling condition, higher f_{rep} and larger Δf_{rep} can effectively improve the acquisition speed for dynamic measurements of high-speed moving targets [1, 2]. Further research shows that there exists an optimal Δf_{rep} for each f_{rep} where the ranging uncertainty is minimized, achieving the highest precision. With fixed optical spectral bandwidth, a higher f_{rep} corresponds to a larger optimal Δf_{rep} and an even improved ranging precision [3]. As to dual-comb spectroscopy, likewise a larger Δf_{rep} can effectively reduce acquisition time, thereby improving measurement speed [4, 5]. This is significant for dynamic applications where timeliness is emphasized, such as during intense chemical reactions or in rapidly moving gas flows [6, 7]. In addition, dual-combs with high f_{rep} and large Δf_{rep} can yield more interferograms for averaging within a fixed time window, favoring improvement of the signal-to-nosie ratio (SNR) [8, 9].

Different with on-chip microresonator-based dual combs which can easily achieve GHz f_{rep} and large Δf_{rep} [10, 11], it has long been challenging to reach the level in fiber laser scheme. The method of short-cavity usually faces the limitation of fiber gain and device integration [12], while electro-optic comb features narrow bandwidth and high cost [13]. Another way is harmonic mode-locking which exploits the multiple pulses in laser cavity [14, 15], yet the trigger of dual harmonic pulse trains in single cavity remains barely explored. However, once achieved, the fiber dual-comb would show salient advantages in budget and efficiency to on-chip dual-comb for sparing the cost of tape-out and precision detuning systems, as well as the long-concerned coupling loss. The high f_{rep} dual-comb fiber laser could also supplement the sub-10 GHz band which is hardly attainable for the microresontors [16, 17].

In this work, a monolithic short-linear-cavity fiber laser integrated with multifunctional device is proposed and demonstrated for generating two sets of harmonic mode-locked pulses through polarization multiplexing. The device, named as fiber-coupled dual-comb mirror (FDCM), serves as a polarization multiplexer and a mode-locker simultaneously. By adjusting the device along with pump power, dual pulse trains mode-locked at varied harmonic orders can be achieved and switched, which should be the first observation of polarization-asymmetric asynchronous harmonic vector solitons in fiber, to the best of our knowledge. At the frequency of the least common multiple (LCM) of the harmonic orders, the equivalent Δf_{rep} of the dual harmonic comb can be multiplied, leading to more interferograms within the same sampling window for dual-comb acquisition rate multiplication, revealing a low-cost, low-complexity solution to high-speed measurement scenarios.

Principle

The polarization-multiplexed dual-comb laser is constructed with a monolithic Fabry–Perot fiber cavity, as shown in Fig. 1a, which mainly consists of a distributed Bragg reflector (DBR), an erbium-doped fiber (EDF), and the core functional part FDCM. The gain fiber gets pumped by a 974 nm laser diode through wavelength division multiplexer (WDM) and the generated combs are extracted from the cavity via DBR layer. The polarization controller (PC) 1 in the cavity is employed to regulate the intra-cavity polarization state of the laser, and the PC 2 in output optical path works with the inline polarization beam splitter (PBS) for detachment of the dual-comb. Polarization-independent isolator (PI-ISO) is also used here to avoid reflection disturbances. The key device FDCM comprises two graded-index (GRIN) lenses for collimation and focusing, one Bi-crystal for polarization multiplexing, and a commercial semiconductor saturable absorber mirror (SESAM) for mode-locking, as illustrated in Fig. 1b. The design and fabrication details can be found in Supplementary Note 1.

To excite two combs simultaneously in the same cavity, it is necessary that both polarization states reach the mode-locking threshold. Theoretically the laser could only be mode-locked when its optical intensity I ($=P/A$, where P denotes optical power and A denotes mode-filed area) reaches the saturation threshold of saturated absorber (SA), which requires a reasonable distribution of energy between the two polarizations by adjusting the intra-cavity optical elements.

The most direct factor is tuning the power distribution between two polarizations. Since the pump we use is linearly polarized, the excited laser should also be linearly polarized. When the laser (P) with arbitrary polarization direction is incident on the surface of the Bi-crystal, as the green-labelled polarization field shown in Fig. 1c, it will be decomposed into two components, P_x and P_y, according to the coordinate angle θ determined by the crystal's axes (XY), and then spatially separated when passing through the crystal (red and blue field in Fig. 1c. The power of two beams can be simply determined by

$$\begin{aligned} P_x &= P\cos^2\theta \\ P_y &= P\sin^2\theta \end{aligned} \tag{1}$$

By tuning the relative angle between the fast axes of fiber and crystal through rotating PC 1 or Bi-crystal, θ will change accordingly and the relative intensity of the decomposed orthogonal-polarized beams will get manipulated (see Supplementary Note 1 and Supplementary Movie 1). If the power of both beams of light with varied optical path meet the mode-locking threshold, they would oscillate simultaneously in the cavity to produce two sets of pulses with different f_{rep}.

Another factor that affects the oscillation and operation regimes of the two polarization states is the mode-field area of the focused beam at SESAM surface. As a focusing-reflecting optical propagation structure, if the SESAM in the FDCM mismatches the focal plane of the focused beam too much, the laser beam fluence will be drastically weakened, resulting in failure of mode-locking. Furthermore, it should be noted that the focal planes of the two mutually orthogonal polarized light passing

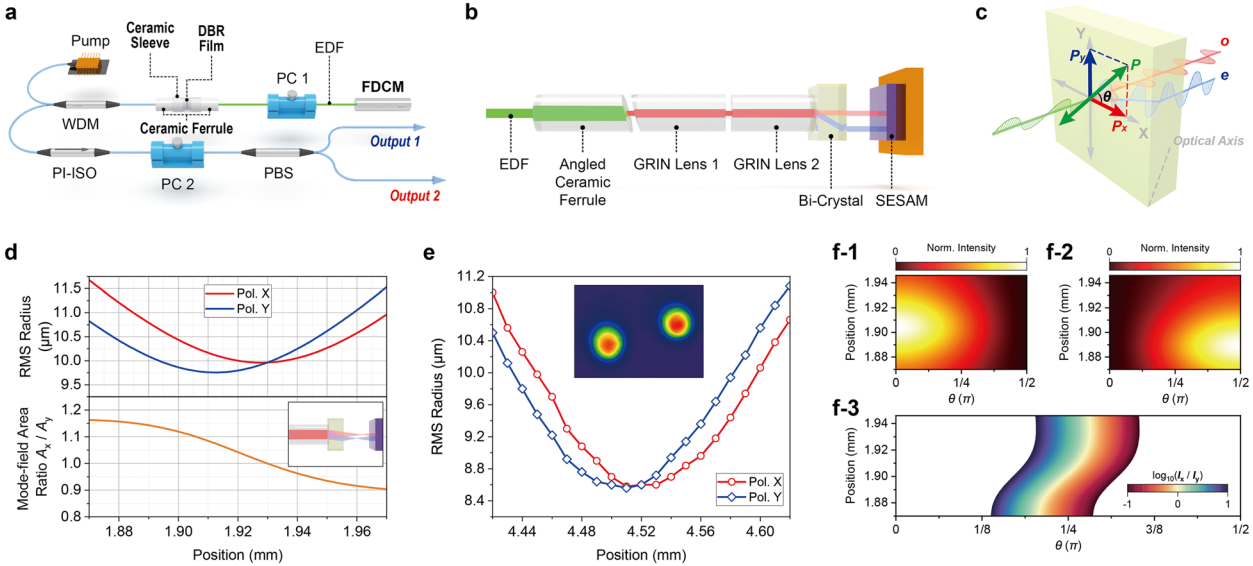

Fig. 1 Principle of the fiber-based harmonic dual-comb. **a** Schematic diagram of the fiber laser setup. **b** Structure of the fiber-coupled dual-comb mirror device. **c** Decomposition schematic of linearly polarized light propagating through a birefringent crystal. **d** Calculated RMS radius of o- and e-beam spots varying with propagating position (upper); Mode field area ratio of the two spots tuned by SESAM position (lower), where the inset shows the schematic diagram of birefringent induced aberration. **e** Variation of the measured spot size with respect to the SESAM position in experiment. The inset shows measured light spots with CCD. Mapping plots of normalized optical intensity as a function of relative polarization angle θ and SESAM position are shown in (**f-1**) for Polarization X and (**f-2**) for Polarization Y; (**f-3**) Mapping plot of the normalized intensity ratio of the two orthogonal polarized beams as a function of θ and SESAM position

through the Bi-crystal do not coincide due to the birefringent aberration, as the simulated root mean square (RMS) radii of the o- and e-light spots varying with position shown in the top panel of Fig. 1d. Owing to the aberration, the mode-field areas for the two beams at SESAM surface can be equal or unequal depending on SESAM position, as illustrated in the Fig. 1d inset. The relative area ratio of the two beams gets tuned accordingly, depicted in the lower panel of Fig. 1d. Using a self-built microscope system [18], we observed the variation of the mode-field diameters of the two spots on different imaging surfaces, and the results in Fig. 1e are consistent with the calculated change tendency. Such tunability of mode-field area offers another degree of freedom to control the optical intensity of each polarization, thus determining the laser operation regime.

Figures 1 f-1 and f-2 show the mapping plots of the normalized optical intensity of the two beams versus the changes of the incident polarization relative angle θ to the crystal coordinate and the position of the SESAM. It can be seen that the optical intensity of o-beam (Pol. X) and e-beam (Pol. Y) vary with θ as cosine function describes but reach maximum at different SESAM locations. This result shows that we can achieve arbitrary proportional distribution and fine adjustment of both beam's optical intensity by tuning these two degrees of freedom, thereby realizing simultaneous mode locking of two polarization states and controlling of the mode-locked pulse energy. The mapping plot of the normalized intensity ratio of the two beams versus the two key parameters is shown in Fig. 1 f-3. When a specific polarization state exhibits energy overflow, it tends to operate under the harmonic mode-locking regime. If both polarization states have energy overflow while the optical intensity distribution between them is imbalanced, different orders of harmonic mode-locking can be stimulated.

Harmonic dual-comb generation

The total length of the monolithic cavity in the experiment was ~ 27.1 cm where the EDF counted for ~ 26.1 cm and FDCM section for ~ 1 cm, corresponding to a fundamental f_{rep} of 383 MHz. The employed high Bi-crystal is a Y-cut 45° lithium niobate crystal with thickness of 1 ± 0.1 mm, whose effective birefringence is derived to be ~ 0.04, introducing a spatial walk-off angle of 1.926° and optical path difference of ~ 0.04 mm between the two orthogonally polarized beams. Thereby, the theoretical Δf_{rep} for fundamental dual-comb is about 40 kHz (detailed calculation in Supplementary Note 1).

Fundamental-harmonic dual-comb

Turning on the pump laser and raising the driven current to 370 mA, with adjusting intracavity PC 1 and locating the SESAM at proper position, the fundamental-repetition-rate dual-comb state was realized. In Figs. 2a-d, two sets of pulse trains could be observed both with periods around 2.61 ns. Here the data for x-polarized state (Pol. X) is labelled red while that of y-polarized state (Pol. Y) is blue. As shown in Figs. 2a and c, comb Pol. X had a center wavelength of 1571.9 nm and a 3 dB bandwidth of 7.31 nm, while that of comb Pol. Y comb was 1571.2 nm and 4.65 nm. The optical spectrum of each comb exhibited a conventional soliton envelope with Kelly sidebands. At specific wavelengths, one comb showed a dip sideband while the other with a peak sideband at the same location, which demonstrates coherent energy exchange between the two

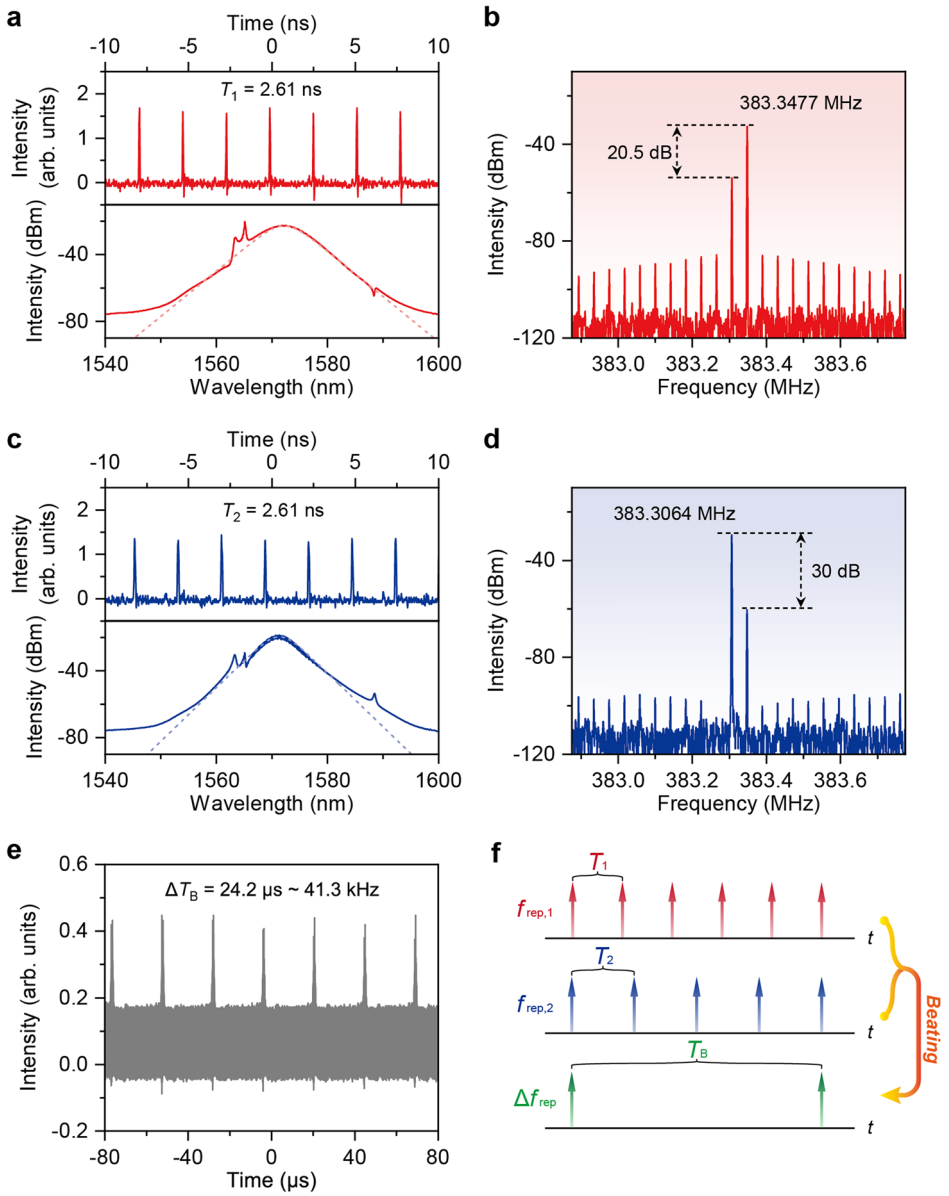

Fig. 2 Characterization of fundamental dual-comb. **a** Oscilloscope trace (top panel) and optical spectrum (lower panel) for comb Pol. X. **b** RF spectrum of comb Pol. X. **c** Oscilloscope trace (top panel) and optical spectrum (lower panel) for comb Pol. Y. **d** RF spectrum of comb Pol. Y. **e** Temporal interferogram of fundamental-rate dual-comb beating. **f** Schematic diagram of sampling process for fundamental-rate dual-comb. The dashed curves in optical spectrum plots represent sech^2 envelope fitting

polarized components [19]. The FWHM durations for pulses of Pol. X and Pol. Y were 2.1 ps and 2.37 ps, respectively, measured by autocorrelator (Supplementary Note 5). The RF spectrum in Fig. 2b and Fig. 2d show that the two main frequency components located at 383.3477 MHz and 383.3064 MHz respectively, with a Δf_{rep} of 41.3 kHz. By adjusting PC 2 before PBS, the Pol. X component at the fundamental frequency achieved an extinction ratio of 20.5 dB, and Pol. Y reached 30 dB, proving that they were dual-combs with orthogonal polarization. The SNR for both frequency components exceeded 70 dB. After the separated combs re-encountered in a 50:50 optical fiber coupler and

beat in a balanced photodetector (BPD), comb Pol. Y performed temporal asynchronous sampling on comb Pol. X in time-domain, and the periodic interferograms were obtained as shown in Fig. 2e. The beat note interval is about 24.2 μs, which corresponds to the frequency difference in RF domain. Figure 2f illustrates the sampling process of the two fundamental-rate combs. The sampling pulse (with repetition rate $f_{\mathrm{rep},1}$ and time period T_1) and signal pulse (with repetition rate $f_{\mathrm{rep},2}$ and time period T_2) experience periodic overlapping and dislocating in time domain due to different repetition rates, forming cross correlation interference signal in every measurement period $T_{\mathrm{B}} = 1/\Delta f_{\mathrm{rep}}$, which corresponds to multimode heterodyne interference in frequency domain.

Next, by fine-tuning the intra-cavity PC 1 and increasing the pump current, the comb Pol. Y evolved into a harmonic mode-locking regime while the comb Pol. X remained pulsing at fundamental rate. Here we obtained the equivalent Δf_{rep} of 85.6 kHz and 120.3 kHz for the 2nd-order-harmonic and 3rd-order-harmonic comb Pol. Y, under pump current of 450 mA and 510 mA, respectively. More cases of dual-comb under such regime can be found in Supplementary Note 3. Keeping the pump current at 510 mA and tuning PC 1, the power of two polarizations was re-distributed, where a dual-comb output consisting of fundamental rate and 4th-order harmonic was obtained, and the detached pulse trains, optical spectrum, and RF spectrum are demonstrated in Fig. 3a-f (Spectral and temporal details in Supplementary Note 5). Due to the rotating of PC 1, fiber birefringence was added, lifting the fundamental rate to 44.8 kHz. The main frequency components of the two polarizations at 4th harmonic were 1533.4307 MHz and 1533.2518 MHz with equivalent Δf_{rep} of 178.9 kHz, which is about 4 times of fundamental Δf_{rep} at this stage. The RF extinction ratios between the two repetition rates were relatively degraded here, as depicted in Fig. 3c and f. One incentive is the large difference between the optical power of the fundamental-rate Pol. X and the 4th-order-harmonic Pol. Y, which directly determines the RF spectral power. In addition, harmonic pulses bring more chances for the nonlinear interaction between co- and counter-propagating fields in the linear cavity [20], inducing stronger cross-phase modulation and polarization rotation of each comb, causing the crosstalk. The extinction ratio could be further optimized by introducing spectral reshaping scheme to limit pulse peak power for restraint of nonlinear interaction and rotation [21].

For the harmonic operation in Pol. Y, the peak intensity of pulse train exhibited fluctuations as a result of supermode noise, which manifests as other harmonic components in Fig. 3e. Here the supermode suppression ratio (SMSR) reached 29.8 dB for 4th harmonic. The further mitigation methods and influence on dual-comb metrology are discussed in Supplementary Note 6. The corresponding beat note interval is reduced to 5.6 μs as well (Fig. 3g). Here utilizing the equivalent sampling process (Supplementary Note 2), it is easier to understand the multiplication process. As shown in Fig. 3h, it can be regarded that N sets of pulses (here depicts 4 for example) with repetition rate $f_{\mathrm{rep},2}$ and equal time delay (which is just the $1/N$ of fundamental period T_2) all get sampled by the comb with fundamental-rate $f_{\mathrm{rep},1}$. As a result, the sampling period is shortened by N times compared to that in Fig. 2f. In our experiment, up to 6th-order-harmonic comb Pol. Y emerged while comb Pol. X stayed fundamental (Supplementary Note 3).

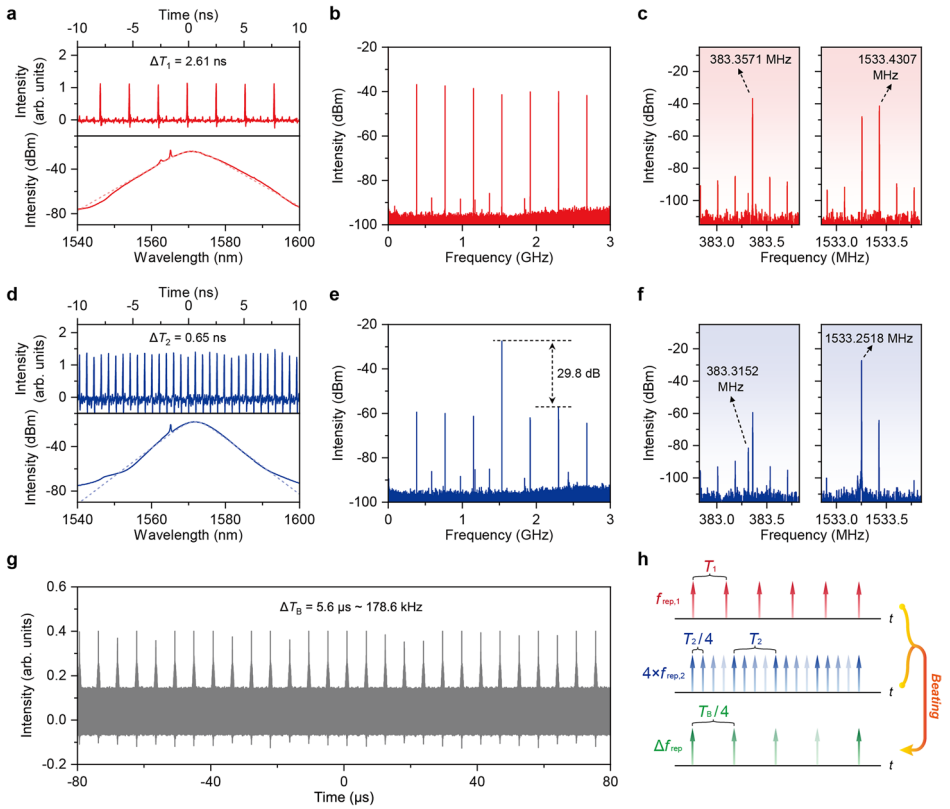

Fig. 3 Characterization of fundamental-harmonic dual-comb. **a** Oscilloscope trace (top panel) and optical spectrum (lower panel) for comb Pol. X. **b** RF spectrum of comb Pol. X within 3 GHz range. **c** Local RF-spectral scanning of comb Pol. X around fundamental frequency (left panel) and 4th-order harmonic (right panel). **d** Oscilloscope trace (top panel) and optical spectrum (lower panel) for comb Pol. Y. **e** RF spectrum of comb Pol. Y within 3 GHz range. **f** Local RF-spectral scanning of comb Pol. Y around fundamental frequency (left panel) and 4th-order harmonic (right panel). **g** Temporal interferogram of fundamental and 4th-order-harmonic dual-comb beating. **h** Schematic diagram of sampling process for fundamental and 4th-order-harmonic dual-comb. The dashed curves in optical spectrum plots represent $sech^2$ envelope fitting

Dual-harmonic-comb

Owing to the low saturation fluence of the SESAM utilized in the FDCM device and multiple tuning flexibility, the laser is also capable of generating polarization multiplexed dual-combs which are both harmonic mode-locked (details of SESAM and incident optical fluence are in Supplementary Note 7). At the pump current of 470 mA, by adjusting PC 1 and the distance between the SESAM and the Bi-crystal, dual 2nd-harmonic mode-locking combs were realized. The pulse trains, optical spectrum, and RF spectrum of the two separated 2nd-order-harmonic mode-locked outputs can be found in Fig. 4a-f (details in Supplementary Note 5). Oscilloscope traces demonstrate the stabilized pulse trains for each comb separately, and the spectral shapes indicated conventional soliton which can be ideally fitted by $sech^2$ envelope as well. The RF spectrum show that the two main frequency components located at 766.6879 MHz and 766.6027 MHz, respectively, yielding an equivalent Δf_{rep} of 85.2 kHz at the 2nd-order harmonic frequency, which is about twice of the intrinsic Δf_{rep} of 42.5 kHz at fundamental rate. The SMSR reached 29.7 dB for Pol. X and 28.3 dB for Pol. Y. The detached dual 2nd-order-harmonic combs were also introduced simultaneously into the fiber coupler, and the beat note interval

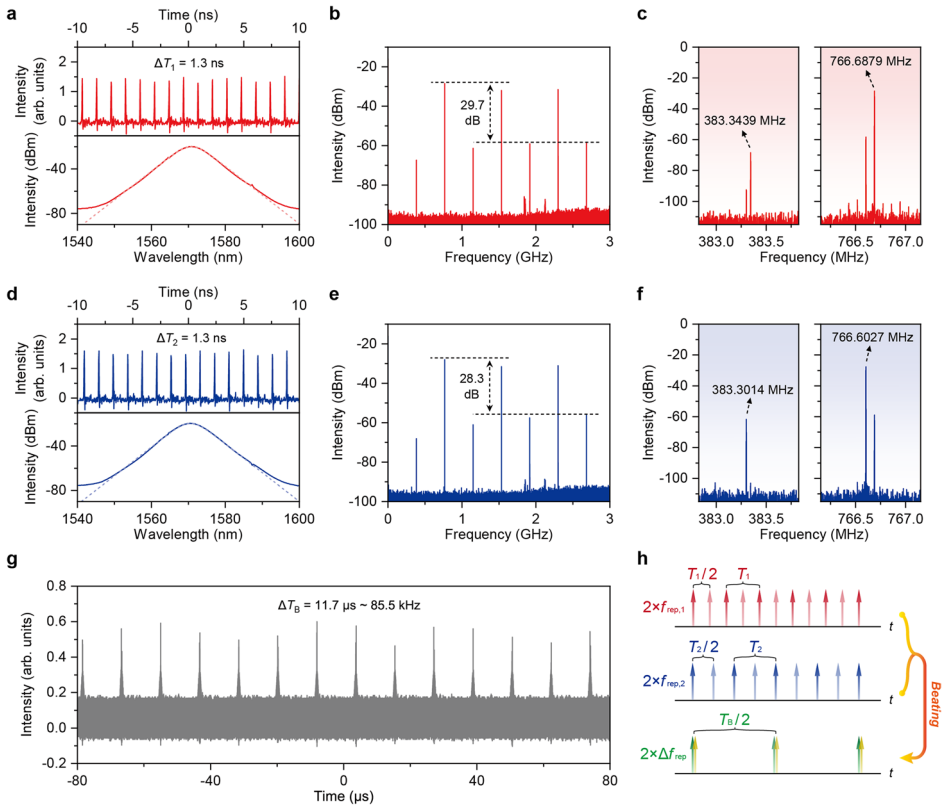

Fig. 4 Characterization of dual-harmonic-comb with identical orders. **a** Oscilloscope trace (top panel) and optical spectrum (lower panel) for comb Pol. X. **b** RF spectrum of comb Pol. X within 3 GHz range. **c** Local RF-spectral scanning of comb Pol. X around fundamental frequency (left panel) and 2nd-order harmonic (right panel). **d** Oscilloscope trace (top panel) and optical spectrum (lower panel) for comb Pol. Y. **e** RF spectrum of comb Pol. Y within 3 GHz range. **f** Local RF-spectral scanning of comb Pol. Y around fundamental frequency (left panel) and 2nd-order harmonic (right panel). **g** Temporal interferogram of dual 2nd-order-harmonic-comb beating. **h** Schematic diagram of sampling process for dual 2nd-order-harmonic combs. The dashed curves in optical spectrum plots represent sech^2 envelope fitting

between the interference peaks is about 11.7 μs in Fig. 4g, which is equivalent to $1/(2\Delta f_{\text{rep}})$. The identical order harmonic comb sampling process is shown in Fig. 4h, where N sets of signal pulses (here 2 for example) with $f_{\text{rep},2}$ and equal time delay of T_2/N get sampled by N sets of sampling pulse with $f_{\text{rep},1}$ and equal time delay of T_1/N sequentially. Because of the same harmonic order, the sampling results tend to overlap and the equivalent Δf_{rep} is approximately equal to the fundamental-N-order-harmonic situation (Supplementary Note 2).

With the pump current set back to 510 mA, the two polarization states of the dual-comb laser underwent harmonic order change. The enhanced energy in cavity caused one of the 2nd-order-harmonic channels to take the lead up to 3rd-order-harmonic mode-locking, as exhibited in Fig. 5a-f. The oscilloscope traces show the stable pulse train of each comb respectively which could be observed asynchronously in the temporal domain. The comb Pol. X exhibited SMSR of 26.6 dB at 2nd harmonic (Fig. 5b), while that of the comb Pol. Y was 26.4 dB at 3rd harmonic (Fig. 5e). At the 6th-order-harmonic frequency, the two main frequency components at 2300.0539 MHz and 2299.8094 MHz differed by ~ 244.5 kHz, a nearly sixfold enhancement relative to the

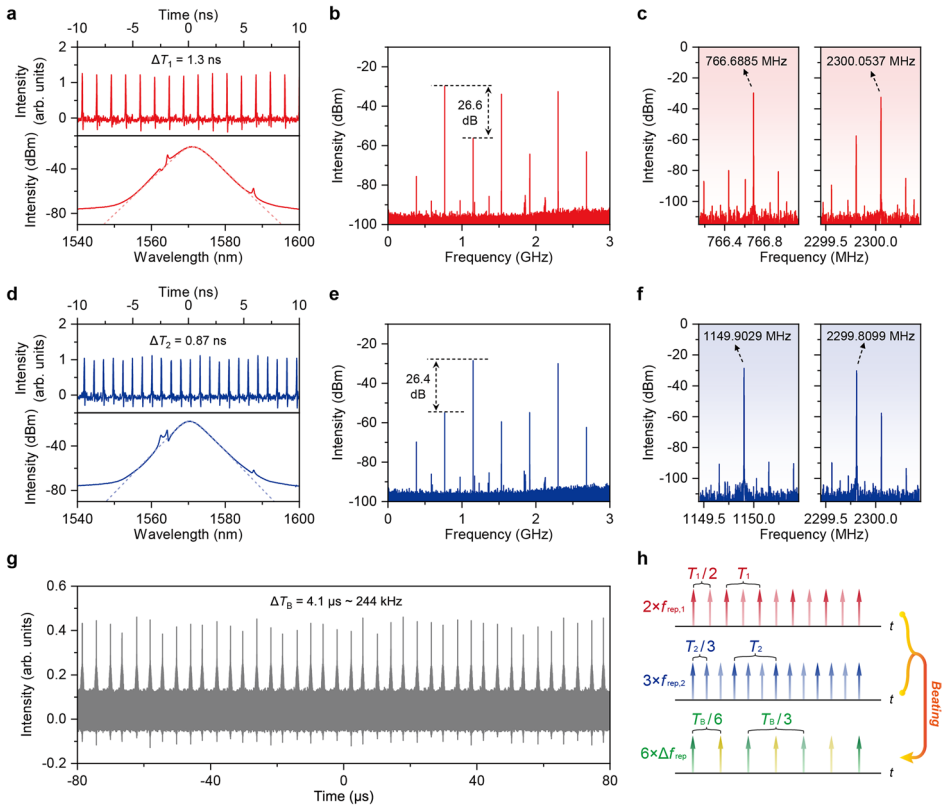

Fig. 5 Characterization of dual-harmonic-comb with coprime orders. **a** Oscilloscope trace (top panel) and optical spectrum (lower panel) for comb Pol. X. **b** RF spectrum of comb Pol. X within 3 GHz range. **c** Local RF-spectral scanning of comb Pol. X around 2nd-order harmonic (left panel) and 6th-order harmonic (right panel). **d** Oscilloscope trace (top panel) and optical spectrum (lower panel) for comb Pol. Y. **e** RF spectrum of comb Pol. Y within 3 GHz range. **f** Local RF-spectral scanning of comb Pol. Y around 3rd-order harmonic (left panel) and 6th-order harmonic (right panel). **g** Temporal interferogram of 2nd- and 3rd-order-harmonic dual-comb beating. **h** Schematic diagram of sampling process for 2nd- and 3rd-order-harmonic dual-comb. The dashed curves in optical spectrum plots represent sech^2 envelope fitting

Δf_{rep} at the fundamental-frequency. In Fig. 5g, the interference period is about 1/6 of the fundamental-frequency dual-comb beating period. In simple terms, six times the number of interferometric signals in the same time window can be acquired for considerably increasing the acquisition rate and measurement speed for dual-comb ranging or spectral analysis via adopting such cross-sampling mechanism for the dual harmonic pulse trains. By adjusting PC 2 before PBS, the Pol. X component at the sixth-order-harmonic achieved an extinction ratio of 24 dB and 26 dB for Pol. Y, revealing that the two generated combs were nearly orthogonally polarized, with SNR exceeding 60 dB for both frequencies. The sampling process of dual harmonic combs with coprime orders is shown in Fig. 5h, where N sets of signal pulses (here 3 for example) with $f_{\text{rep},2}$ and equal time delay of T_2/N get sampled by M sets of sampling pulse with $f_{\text{rep},1}$ and equal time delay of T_1/M sequentially. Since the sampling results do not overlap, the beating signals get arranged orderly with rate multiplied by least common multiple of M and N (also see Supplementary Note 2). In experiments, other dual-harmonic cases were also observed, as demonstrated in Supplementary Note 4.

Discussion

As demonstrated, adequate allocation of optical intensity into orthogonal states by tuning intracavity polarization and beam spot sizes plays the key role to boost controllable harmonic dual-comb in our laser setup, while pump level determines the upper limit of harmonic orders. For fiber lasers with cavity operating in the anomalous dispersion regime, the optical pulse will evolve into a conventional soliton owing to the balance of dispersion and self-phase modulation. With pulse energy of certain polarization increasing, the modulation instability due to nonlinear effects and the lower saturated fluence of the SA adopted in experiments will result in splitting of the laser pulse, such that multiple pulses are generated [22]. These pulse sequences circulating in the cavity will coherently drive acoustic vibrations in the fiber, and when an integer multiple of the frequency of the *N*th harmonic mode-locking is located near the peak of the opto-mechanical gain, the excited mechanical resonance traps each pulse in the sequence within a single acoustic vibration cycle, and the *N* pulses are consequently uniformly distributed in the laser cavity [23]. The polarization multiplexed asynchronous pulse trains with distinct power and intensity experience different nonlinear optical and acoustic processes, thereby splitting into different numbers of sub-pulses and stimulating different acoustic resonance. Therefore, the dual combs get mode-locked at (*M*, *N*)-order harmonic respectively, where the integer *M* and *N* can be equal or not. Considering the minimal dispersion and nonlinearity accumulated in the air and birefringent crystals, the generated dual-comb in this setup can still be regarded as fiber solitons. The vector characteristics of passive harmonic mode-locking solitons in fiber lasers have long been studied, yet most observations and discussions focused on synchronized pulses, where the two polarization solitons had the same harmonic order and repetition rate [14, 19, 24–28]. Therefore, the laser output boosted by FDCM in this setup should be an exemplary observation of polarization-asymmetric harmonic asynchronous vector solitons in fiber, where pulses belonging to two polarizations have different repetition rates and can also present different harmonic orders. The dynamic picture of photoacoustic coupling in the same fiber that involves two asynchronous polarization-multiplexed optical pulses is quite fascinating.

The laser setup was turned on from pump = 0 mW with FDCM settings unchanged to testify the self-start capability. The average output power of the laser varied with pump under different harmonic regimes can be seen in Fig. 6a. For the fundamental and 4th-harmonic dual-comb state, the laser realized unstable fundamental mode-locking at the pump power of 214 mW. When the pump increased to 273 mW, the output of Pol. Y eventually evolved into stable 4th-harmonic mode-locking while Pol. X delivered steady fundamental-rate pulse train. The Pol. X had a slope efficiency of 0.33% and the Pol. Y had 1.03%. At the final dual-comb state, the average power of Pol. Y was about 3.1 times that of Pol. X. Here we label the intermediate unstable state as transition region. For 2nd- and 3rd-harmonic dual-comb regime, the transition region exhibited more drastic jittering, as shown in lower panel of Fig. 6a. It can be observed from the curves that energy fluctuation and exchange exist in this pump-power interval, until the dual-comb threshold is reached and the two stable combs are established at the same time. In this state, the transition region spanned over pump power from 194 to 333 mW. Averaged

slope was 0.6% for Pol. X and 0.82% for Pol. Y, while the average power ratio was 1.36 between Pol. Y and Pol. X at the dual-comb regime.

To further testify the coherence of the generated GHz harmonic dual-comb, multi-mode heterodyne interference results of the detached dual combs are measured in experiments. Take the 2nd- and 3rd-order harmonic dual-comb as a typical case, shown in upper part of Fig. 6a, clear interferometric signal measured with BPD can be observed after low-pass filtering. A total of 244.5 thousand peaks of interferograms can be acquired in 1 s, and the high sampling rate bid fair to facilitate fast ranging and spectral analysis applications. The lower part of Fig. 6a provides a magnified view of the interferogram, demonstrating clear interference fringes. As to the frequency domain, the lower part of Fig. 6b demonstrates the typical Fourier transform of the temporal interferogram, which is captured with dual 3rd-order harmonic comb. The corresponding optical spectrum of the comb depicted in the upper part shows conspicuous down-conversion in the RF domain. The zoom-in view in the middle inset of Fig. 6b shows the RF comb with interval of about 131 kHz. The common mode rejection endowed by the sharing cavity ensures the comb-line resolved teeth with SNR over 20 dB.

In order to investigate the stability of the harmonic dual-comb operation, the f_{rep} of the two mode-locked pulse trains and their Δf_{rep} were monitored by continuously scanning the RF spectrum. Figure 6d records the drift of f_{rep} and Δf_{rep} over a 3-min period for the two orthogonally polarized outputs of dual third-order-harmonic comb. In the absence of any environmental control (e.g., temperature control and frequency stabilization), there is more pronounced fluctuation in the f_{rep} of the two polarizations, with standard deviations of ~ 1778.0152 Hz and 1775.0624 Hz, respectively. However, since the combs circulate in the same cavity and are pumped by the same source, the f_{rep} drift of the two polarizations has a similar tendency, which results in the Δf_{rep} being much more stable than the f_{rep} itself, thanks to the common mode rejection. A standard deviation of 36.64 Hz for the change of Δf_{rep} over a 3-min time span is achieved, which implies that the short-term absolute fluctuation of the dual GHz-harmonic comb equivalent Δf_{rep} is lower than 0.029%. We further measured the 40-min long-term stability of the harmonic dual-comb, as shown in Fig. 6e. The standard deviations of the frequency drift for the two repetition rates are 2349.3 Hz and 2344.3 Hz, respectively, while the standard deviation of the Δf_{rep} is only 44.42 Hz, maintaining good stability. All the achieved dual-harmoinc combs show steady operation without manual adjustment and no hopping between different harmonic orders gets observed (Supplementary Note 8). In addition, the certain dual-harmonic-comb can be retrieved after repeated switching of pump as long as the setup remaining unchanged (Supplementary Movie 2). By recording the data of pump power, PC angle and SESAM position as calibration, harmonic orders can also be nimbly shifted so as to control the equivalent Δf_{rep} of laser output (Supplementary Movie 3).

In our experiments, the maximum equivalent Δf_{rep} reached up to 399.375 kHz in the same setup with further shrunken gain fiber and a higher harmonic f_{rep} of 3.052 GHz (see Supplementary Note 9 for details), which, to the best of our knowledge, is the highest record currently available in the field of fiber-based single cavity dual-combs, as illustrated in Fig. 7. By optimizing the integrated spatial optical components for more

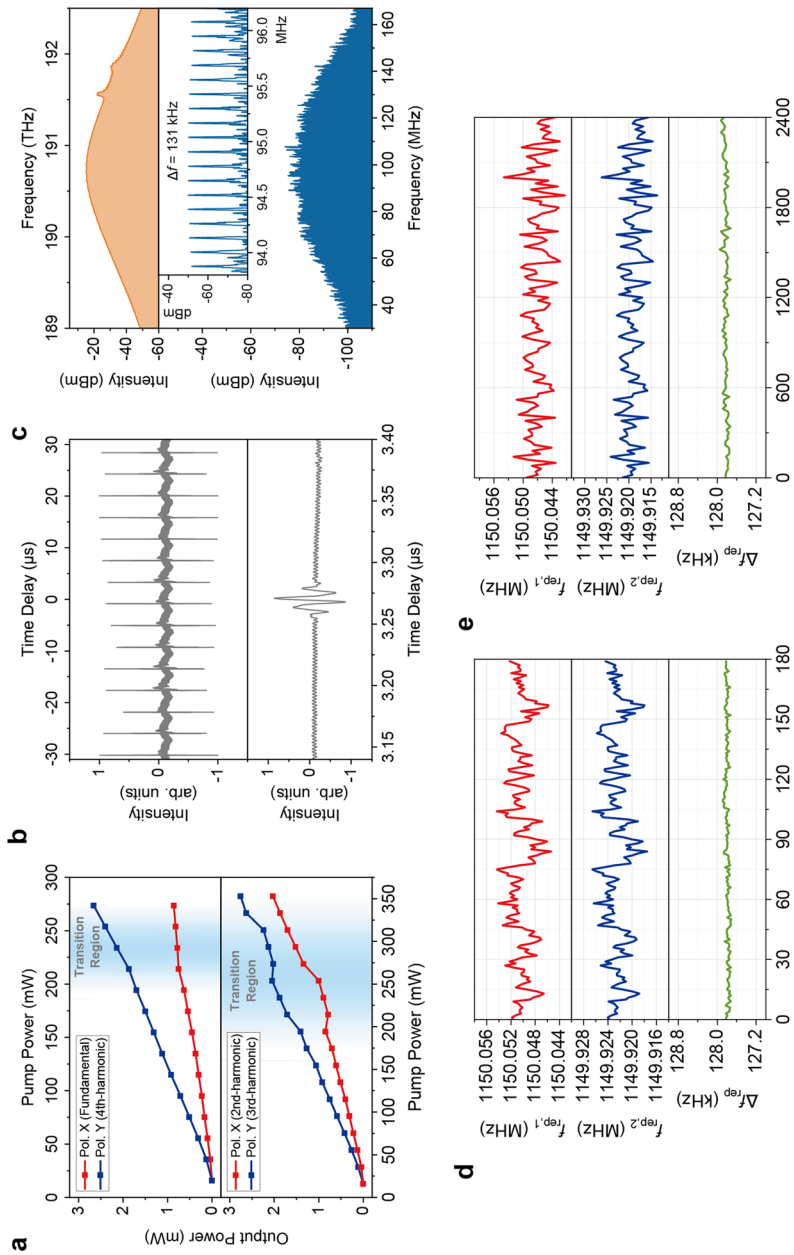

Fig. 6 **a** Average output power of the laser versus pump power under the states corresponding to fuandamental-4th-harmonic dual-comb (top) and 2nd-3rd-harmonic dual-comb (lower). **b** Interferogram with frequency of 244.5 kHz captured by BPD (upper) and zoomed-in figure of the interference signal (lower). **c** Typical Fourier-transformed interferogram in the RF-spectrum domain with local zoom within 2.5 MHz span in the inset (center), and corresponding optical spectrum (top). **d** f_{rep} and Δf_{rep} stability of third-order-harmonic dual-comb for 3 min and (**e**) for 40 min

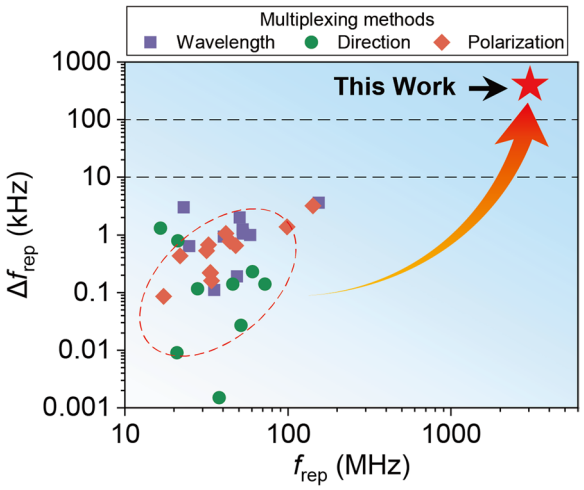

Fig. 7 A summary of f_{rep} and Δf_{rep} for different fiber single-cavity dual-comb lasers based on wavelength-multiplexing [29–38], direction-multiplexing [39–47], and polarization-multiplexing [48–59]

compact packaging and external interventions, this laser scheme shows the potential to further increase the speed of dual-comb measurements.

Conclusion

In conclusion, we demonstrate a linear-cavity monolithic fiber laser incorporating fiber-coupled multifunctional device for generation of GHz harmonic dual combs. The proposed structure integrates GRIN lenses, Bi-crystal and SESAM functions as collimator, polarization multiplexer, and saturable absorber simultaneously, showing the advantages of small size, low complexity and low cost. The fundamental/harmonic dual-combs with varied repetition-rate differences are generated by tuning the angle-off between laser beam polarization in gain fiber and axis of birefringent crystal, along with the relative position of SESAM. Stable dual-comb output with a repetition rate up to 383 MHz and an equivalent repetition rate difference of 244.5 kHz is obtained based on harmonic cross-sampling, while the utmost experimental demonstration reaches 509 MHz repetition rate and near 400 kHz rate difference, achieving the highest repetition rate difference reported for fiber-based single-cavity dual-comb laser. The single-linear-cavity fiber laser is believed to provide a compact and convenient solution for improving the acquisition speed and accuracy of dual-comb measurements in extensive application fields such as chemical substance composition analysis, ranging, and environmental monitoring.

Abbreviations

OFC	Optical frequency comb
f_{rep}	Repetition rate
Δf_{rep}	Repetition rate frequency difference
SNR	Signal to noise ratio
Bi-crystal	Birefringent crystal
FDCM	Fiber-coupled dual-comb mirror
LCM	Least common multiple
DBR	Distributed Bragg reflector
EDF	Erbium-doped fiber
WDM	Wavelength division multiplexer
PC	Polarization controller
PBS	Polarization beam splitter
PI-ISO	Polarization-independent isolator

GRIN	Graded-index
SESAM	Semiconductor saturable absorber mirror
SA	Saturated absorber
RMS	Root mean square
BPD	Balanced photodetector

Supplementary Information

The online version contains supplementary material available at https://doi.org/10.1186/s43074-025-00161-y.

Supplementary Material 1

Supplementary Material 2

Supplementary Material 3

Supplementary Material 4

Acknowledgements
Not applicable.

Authors' contributions
Wang G and Ding Z contributed equally to this work. Xu F and Ding Z conceived the idea and initiated the project. Wang G and Ding Z wrote the manuscript, produced the figures, and contributed to the experimental results. Ding Z and Wang G edited the manuscript. Xu F supervised the project. All authors read and approved the final manuscript.

Funding
This work was supported by the National Natural Science Foundation of China (61925502, 62135007 and 62405130), Natural Science Foundation of Jiangsu Province (BK20243014), Guangdong Basic and Applied Basic Research Foundation(2023B1515120011), National Key R&D Program of China (2021YFA1401103), and Innovation Program for Quantum Science and Engineering (2021ZD0300700). We also acknowledge support from China Postdoctoral Science Foundation (2023M741619) and Postdoctoral Fellowship Program of CPSF (GZC20231099).

Data availability
The data that support the fundings of this study are available from the corresponding author upon reasonable request.

Declarations

Competing interests
The authors declare that they have no competing interests.

Received: 7 November 2024 Revised: 25 January 2025 Accepted: 1 February 2025
Published online: 20 February 2025

References

1. Trocha P, Karpov M, Ganin D, Pfeiffer MHP, Kordts A, Wolf S, Krockenberger J, Marin-Palomo P, Weimann C, Randel S, Freude W, Kippenberg TJ, Koos C. Ultrafast optical ranging using microresonator soliton frequency combs. Science. 2018;359:887–91.
2. Mitchell T, Sun JH, Reid DT. Dynamic measurements at up to 130-kHz sampling rates using Ti:sapphire dual-comb distance metrology. Opt Express. 2021;29:42119–26.
3. Wu GH, Xiong SL, Ni K, Zhu ZB, Zhou Q. Parameter optimization of a dual-comb ranging system by using a numerical simulation method. Opt Express. 2015;23:32044–53.
4. Fortier T, Baumann E. 20 years of developments in optical frequency comb technology and applications. Commun Phys. 2019;2:153.
5. Dutt A, Joshi C, Ji XC, Cardenas J, Okawachi Y, Luke K, Gaeta AL, Lipson M. On-chip dual-comb source for spectroscopy. Sci Adv. 2018;4: e1701858.
6. Long DA, Cich MJ, Mathurin C, Heiniger AT, Mathews GC, Frymire A, Rieker GB. Nanosecond time-resolved dual-comb absorption spectroscopy. Nat Photonics. 2024;18:127–31.
7. Hoghooghi N, Chang PT, Egbert S, Burch M, Shaik R, Diddams SA, Lynch P, Rieker GB. GHz repetition rate mid-infrared frequency comb spectroscopy of fast chemical reactions. Optica. 2024;11:876–82.
8. Yu H, Qian Z, Xinghui L, Wang X, Ni K. Phase-stable repetition rate multiplication of dual-comb spectroscopy based on a cascaded Mach-Zehnder interferometer. Opt Lett. 2021;46:3243–6.
9. Hoghooghi N, Cole RK, Rieker GB. 11-μs time-resolved, continuous dual-comb spectroscopy with spectrally filtered mode-locked frequency combs. Appl Phys B-Lasers O. 2021;127:17.
10. Lucas E, Lihachev G, Bouchand R, Pavlov NG, Raja AS, Karpov M, Gorodetsky ML, Kippenberg TJ. Spatial multiplexing of soliton microcombs. Nat Photonics. 2018;12:699–705.
11. Zhang H, Tan T, Chen HJ, Yu Y, Wang WT, Chang B, Liang YP, Guo YH, Zhou H, Xia HD, Gong QH, Wong CW, Rao YJ, Xiao YF, Yao BC. Soliton Microcombs Multiplexing Using Intracavity-Stimulated Brillouin Lasers. Phys Rev Lett. 2023;130: 153802.

12. Chen XW, Lin W, Hu X, Wang WL, Liang ZH, Ling L, Yang Y, Guo YK, Liu T, Chen DD, Wei XM, Yang ZM. Dynamic gain driven mode-locking in GHz fiber laser. Light Sci Appl. 2024;13:265.
13. Carlson DR, Hickstein DD, Cole DC, Diddams SA, Papp SB. Dual-comb interferometry via repetition rate switching of a single frequency comb. Opt Lett. 2018;43:3614–7.
14. Sergeyev S, Kolpakov S, Loika Y. Vector harmonic mode-locking by acoustic resonance. Photonics Res. 2021;9:1432–8.
15. Yeh DH, He WB, Pang M, Jiang X, Russell PS. Synchronization of gigahertz core resonances in multiple photonic crystal fiber cores by timing-modulated harmonic mode locking. Optica. 2021;8:1581–5.
16. Kippenberg TJ, Spillane SM, Vahala KJ. Kerr-nonlinearity optical parametric oscillation in an ultrahigh-Q toroid microcavity. Phys Rev Lett. 2004;93: 083904.
17. Pasquazi A, Peccianti M, Razzari L, Moss DJ, Coen S, Erkintalo M, Chembo YK, Hansson T, Wabnitz S, Del'Haye P, Xue XX, Weiner AM, Morandotti R. Micro-combs: A novel generation of optical sources. Phys Rep. 2018;729:1–81.
18. Li Q, Chambonneau M, Blothe M, Gross H, Nolte S. Flexible, fast, and benchmarked vectorial model for focused laser beams. Appl Opt. 2021;60:3954–63.
19. Song YF, Li L, Zhang H, Shen DY, Tang DY, Loh KP. Vector multi-soliton operation and interaction in a graphene mode-locked fiber laser. Opt Express. 2013;21:10010–8.
20. Xiao Z, Wu K, Tieying Li, Chen J. Deterministic single-soliton generation in a graphene-FP microresonator. Opt Express. 2020;28:14933–47.
21. Deng Z, Liu Y, Ouyang C, Zhang W, Wang C, Li W. Mutually coherent dual-comb source generated from a free-running linear fiber laser. Results Phys. 2019;14: 102364.
22. Boguslawski J, Sobon G, Zybala R, Sotor J. Towards an optimum saturable absorber for the multi-gigahertz harmonic mode locking of fiber lasers. Photonics Res. 2019;7:1094–100.
23. Liu X, Pang M. Revealing the Buildup Dynamics of Harmonic Mode-Locking States in Ultrafast Lasers. Laser Photonics Rev. 2019;13:1800333.
24. Luo YY, Li L, Liu DM, Sun QZ, Wu ZC, Xu ZL, Tang DY, Fu SN, Zhao LM. Group velocity locked vector dissipative solitons in a high repetition rate fiber laser. Opt Express. 2016;24:18718–26.
25. Han MM, Zhang SM, Li XL, Zhang HX, Yang H, Yuan T. Polarization dynamic patterns of vector solitons in a graphene mode-locked fiber laser. Opt Express. 2015;23:2424–35.
26. Akosman AE, Zeng JJ, Samolis PD, Sander MY. Polarization Rotation Dynamics in Harmonically Mode-Locked Vector Soliton Fiber Lasers. IEEE J Sel Top Quantum Electron. 2018;24:1101107.
27. Kbashi HJ, Sergeyev SV, Al-Araimi M, Rozhin A, Korobko D, Fotiadi A. High-frequency vector harmonic mode locking driven by acoustic resonances. Opt Lett. 2019;44:5112–5.
28. Tang DY, Zhang H, Zhao LM, Wu X. Observation of High-Order Polarization-Locked Vector Solitons in a Fiber Laser. Phys Rev Lett. 2008;101: 153904.
29. Zhu Y J, Cui Z K, Sun X N, Jiang H B, Zhao H W, Jin L, Yamashita S, Set S Y. All-polarization-maintaining dual-wavelength mode-locked fiber laser based on macro-bending loss tuning. 2020 Conference on Lasers and Electro-Optics (Cleo) 2020:SW3R.3.
30. Hu G, Pan Y, Zhao X, Yin S, Zhang M, Zheng Z. Asynchronous and synchronous dual-wavelength pulse generation in a passively mode-locked fiber laser with a mode-locker. Opt Lett. 2017;42:4942–5.
31. Zhao K, Jia H, Wang P, Guo J, Xiao X, Yang C. Free-running dual-comb fiber laser mode-locked by nonlinear multimode interference. Opt Lett. 2019;44:4323–6.
32. Zhao X, Hu G, Zhao B, Li C, Pan Y, Liu Y, Yasui T, Zheng Z. Picometer-resolution dual-comb spectroscopy with a free-running fiber laser. Opt Express. 2016;24:21833–45.
33. Fellinger J, Mayer AS, Winkler G, Grosinger W, Truong GW, Droste S, Li C, Heyl CM, Hartl I, Heckl OH. Tunable dual-comb from an all-polarization-maintaining single-cavity dual-color Yb:fiber laser. Opt Express. 2019;27:28062–74.
34. Chen J, Nitta K, Zhao X, Mizuno T, Minamikawa T, Hindle F, Zheng Z, Yasui T. Adaptive-sampling near-Doppler-limited terahertz dual-comb spectroscopy with a free-running single-cavity fiber laser. Adv Photonics. 2020;2: 036004.
35. Lin BK, Zhao X, He MZ, Pan YL, Chen J, Cao SY, Lin YG, Wang Q, Zheng Z, Fang ZJ. Dual-Comb Absolute Distance Measurement Based on a Dual-Wavelength Passively Mode-Locked Laser. IEEE Photonics J. 2017;9:7106508.
36. Hu DT, Wu ZL, Cao H, Shi YY, Li RM, Tian HC, Song YJ, Hu ML. Dual-comb absolute distance measurement of noncooperative targets with a single free-running mode-locked fiber laser. Opt Commun. 2021;482: 126566.
37. Zhao X, Li Q, Yin SY, Chen J, Zheng Z. Dual-Comb Dynamic Interrogation of Fiber Bragg Grating With One Mode-Locked Fiber Laser. IEEE Sens J. 2018;18:6621–6.
38. Li Y, Zhang J, Wu F, Liu GH, Xiao XS. Fast dual-comb spectroscopy based on a dual-wavelength all-fiber ring laser with high repetition rate. Appl Phys Express. 2023;16: 012015.
39. Li B, Xing J, Kwon D, Xie Y, Prakash N, Kim J, Huang S. Bidirectional mode-locked all-normal dispersion fiber laser. Optica. 2020;7:961–4.
40. Mehravar S, Norwood RA, Peyghambarian N, Kieu K. Real-time dual-comb spectroscopy with a free-running bidirectionally mode-locked fiber laser. Appl Phys Lett. 2016;108: 231104.
41. Nakjima Y, Hata Y, Minoshima K. High-coherence ultra-broadband bidirectional dual-comb fiber laser. Opt Express. 2019;27:5931–44.
42. Olson J, Ou YH, Azarm A, Kieu K. Bi-Directional Mode-Locked Thulium Fiber Laser as a Single-Cavity Dual-Comb Source. IEEE Photonics Technol Lett. 2018;30:1772–5.
43. Saito S, Yamanaka M, Sakakibara Y, Omoda E, Kataura H, Nishizawa N. All-polarization-maintaining Er-doped dual comb fiber laser using single-wall carbon nanotubes. Opt Express. 2019;27:17868–75.
44. Zhao X, Zheng Z, Liu Y, Hu GQ, Liu JS. Dual-Wavelength, Bidirectional Single-Wall Carbon Nanotube Mode-Locked Fiber Laser. IEEE Photonics Technol Lett. 2014;26:1722–5.
45. Kayes MI, Abdukerim N, Rekik A, Rochette M. Free-running mode-locked laser based dual-comb spectroscopy. Opt Lett. 2018;43:5809–12.
46. Nakajima Y, Kusumi Y, Minoshima K. Mechanical sharing dual-comb fiber laser based on an all-polarization-maintaining cavity configuration. Opt Lett. 2021;46:5401–4.

47. Guo JJ, Ding YH, Xiao XS, Kong LJ, Yang CX. Multiplexed static FBG strain sensors by dual-comb spectroscopy with a free running fiber laser. Opt Express. 2018;26:16147–54.
48. Zhao K, Gao C, Xiao X, Yang C. Buildup dynamics of asynchronous vector solitons in a polarization-multiplexed dual-comb fiber laser. Opt Lett. 2020;45:4040–3.
49. Sterczewski ŁA, Przewłoka A, Kaszub W, Sotor J. Computational Doppler-limited dual-comb spectroscopy with a free-running all-fiber laser. APL Photonics. 2019;4: 116102.
50. Zhao X, Li T, Liu Y, Li Q, Zheng Z. Polarization-multiplexed, dual-comb all-fiber mode-locked laser. Photonics Res. 2018;6:853–7.
51. Gu X, Wang G, Li Y, Gong H, Liang Y, Wu T, Wang J, Liu Y. Polarization-multiplexed, single-cavity dual-comb fiber laser based on a birefringent crystal and a saturable absorber. Opt Express. 2023;31:56–64.
52. Zhao K, Gao C, Xiao X, Yang C. Real-time collision dynamics of vector solitons in a fiber laser. Photonics Res. 2021;9:289–98.
53. Guo J, Zhao K, Zhou B, Ning W, Jiang K, Yang C, Kong L, Dai Q. Wearable and Skin-Mountable Fiber-Optic Strain Sensors Interrogated by a Free-Running. Dual-Comb Fiber Laser Adv Opt Mater. 2019;7:1900086.
54. Hu GQ, Zhu LQ, Sun GK, Lu LL, You R, Liu Y, He W, Dong ML. Spectral overlapping single-cavity dual-comb fiber laser with well-controlled repetition rate difference. Appl Phys Lett. 2022;121: 091101.
55. Uyama K, Shirahata T, Jin L, Set SY, Yamashita S. "All-PM dual-comb fiber ring laser using CNT-SA. In Conference on lasers and electro-optics, OSA technical digest. Optica Publishing Group; 2020. paper SW4R.2.
56. Tao JN, Lin QM, Yan L, Hou L, Lu BL, Bao JT. Asynchronous vector solitons based dual-comb in a fiber laser mode-locked by GO-COOH SA. Opt Laser Technol. 2022;154: 108308.
57. Zhao X, Gong Z, Liu Y, Yang Y, Hu G, Zheng Z. Coherent dual-comb mode-locked fiber laser based on a birefringent ring cavity. In frontiers in optics 2015, OSA Technical Digest (online). Optica Publishing Group; 2015. paper FW3C.3.
58. Liu Y, Zhao X, Zhao B, Yao Z, Gong Z, Yasui T, Zhang L, Zheng Z. High-resolution, dual-comb spectroscopy enabled by a polarization-multiplexed, dual-comb femtosecond fiber laser," in Conference on Lasers and Electro-Optics, OSA Technical Digest (online). Optica Publishing Group; 2016. paper AM4K.5.
59. Gong Z, Zhao X, Hu G, Liu J, Zheng Z. Polarization multiplexed, dual-frequency ultrashort pulse generation by a birefringent mode-locked fiber laser," in CLEO: 2014, OSA Technical Digest (online). Optica Publishing Group; 2014. paper JTh2A.20.

Publisher's Note